Research Article | Vol. 8, No. 7 | 1 Jul 2017 | BIOMEDICAL OPTICS EXPRESS 3360
Biomedical Optics EXPRESS

Multiphoton microscopy for label-free identification of intramural metastasis in human esophageal squamous cell carcinoma

JIAN XU,[1,4] DEYONG KANG,[2,4] YAPING ZENG,[1,4] SHUANGMU ZHUO,[1] XIAOQIN ZHU,[1] LIWEI JIANG,[1] JIANXIN CHEN,[1,5] AND JIANGBO LIN[3,6]

[1]*Key Laboratory of OptoElectronic Science and Technology for Medicine of Ministry of Education, Fujian Provincial Key Laboratory of Photonics Technology, Fujian Normal University, Fuzhou 350007, China*
[2]*Department of Pathology, The Affiliated Union Hospital, Fujian Medical University, Fuzhou 350001, China*
[3]*Department of Thoracic Surgery, The Affiliated Union Hospital, Fujian Medical University, Fuzhou 350001, China*
[4]*These authors contributed equally to this work*
[5]*chenjianxin@fjnu.edu.cn*
[6]*135279779@qq.com*

Abstract: For complete removal of cancerous tissue in esophageal squamous cell carcinoma (ESCC), intramural metastasis (IM) should be identified preoperatively or intraoperatively. Here, multiphoton microscopy (MPM) was introduced for label-free identification of IM in the esophageal wall, by a combination of two-photon excited fluorescence (TPEF), second harmonic generation (SHG) imaging, and spectral analysis. Three-dimensional (3D) imaging of the IM region was also performed. Quantitative parameters, including 3D fiber orientation, were measured by 3D-weighted orientation vector summation. Overall, MPM showed the potential to identify IM. With the development of the advanced MPM endoscope, clinical identification of IM by MPM will be possible.

OCIS codes: (190.0190) Nonlinear optics; (190.1900) Diagnostic applications of nonlinear optics.

References and links

1. S. Tsutsui, H. Kuwano, M. Watanabe, M. Kitamura, and K. Sugimachi, "Resection margin for squamous cell carcinoma of the esophagus," Ann. Surg. **222**(2), 193–202 (1995).
2. N. Yuasa, H. Miyake, T. Yamada, K. Oda, Y. Nimura, T. Nagasaka, and T. Hattori, "Prognostic significance of the location of intramural metastasis in patients with esophageal squamous cell carcinoma," Langenbecks Arch. Surg. **389**(2), 122–127 (2004).
3. H. Kato, Y. Tachimori, H. Watanabe, M. Itabashi, T. Hirota, H. Yamaguchi, and T. Ishikawa, "Intramural metastasis of thoracic esophageal carcinoma," Int. J. Cancer **50**(1), 49–52 (1992).
4. H. Kuwano, M. Watanabe, N. Sadanaga, T. Kamakura, T. Nozoe, M. Yasuda, K. Mimori, M. Mori, and K. Sugimachi, "Univariate and multivariate analyses of the prognostic significance of discontinuous intramural metastasis in patients with esophageal cancer," J. Surg. Oncol. **57**(1), 17–21 (1994).
5. H. Ide, T. Ogino, K. Yoshida, Y. Murata, T. Mogi, T. Hayashi, M. Yoshida, A. Yamada, and M. Endo, "Clinic and pathologic study of esophageal cancer with intramural metastasis (in Japanese)," Jpn. J Gastroenterol. Surg. **13**(7), 781–789 (1980).
6. G. Chen, L. Wang, J. Lu, W. Zhu, H. Zhang, J. Chen, S. Zhuo, and J. Yan, "Optical diagnosis for lung cancer using multiphoton imaging," Scanning **35**(6), 362–365 (2013).
7. K. Tilbury and P. J. Campagnola, "Applications of second-harmonic generation imaging microscopy in ovarian and breast cancer," Perspect. Medicin. Chem. **7**, 21–32 (2015).
8. S. W. Perry, R. M. Burke, and E. B. Brown, "Two-photon and second harmonic microscopy in clinical and translational cancer research," Ann. Biomed. Eng. **40**(2), 277–291 (2012).
9. J. W. Birk, M. Tadros, K. Moezardalan, O. Nadyarnykh, F. Forouhar, J. Anderson, and P. Campagnola, "Second harmonic generation imaging distinguishes both high-grade dysplasia and cancer from normal colonic mucosa," Dig. Dis. Sci. **59**(7), 1529–1534 (2014).
10. T. Hashimoto, K. Arai, Y. Yamashita, Y. Iwasaki, and T. Hishima, "Characteristics of Intramural metastasis in gastric cancer," Gastric Cancer **16**(4), 537–542 (2013).

#292808 https://doi.org/10.1364/BOE.8.003360
Journal © 2017 Received 13 Apr 2017; revised 13 Jun 2017; accepted 14 Jun 2017; published 21 Jun 2017

Biomedical Optics EXPRESS

11. J. Xu, D. Kang, M. Xu, S. Zhuo, X. Zhu, and J. Chen, "Multiphoton microscopic imaging of esophagus during the early phase of tumor progression," Scanning **35**(6), 387–391 (2013).
12. R. Cicchi, A. Sturiale, G. Nesi, D. Kapsokalyvas, G. Alemanno, F. Tonelli, and F. S. Pavone, "Multiphoton morpho-functional imaging of healthy colon mucosa, adenomatous polyp and adenocarcinoma," Biomed. Opt. Express **4**(7), 1204–1213 (2013).
13. J. N. Rogart, J. Nagata, C. S. Loeser, R. D. Roorda, H. Aslanian, M. E. Robert, W. R. Zipfel, and M. H. Nathanson, "Multiphoton imaging can be used for microscopic examination of intact human gastrointestinal mucosa ex vivo," Clin. Gastroenterol. Hepatol. **6**(1), 95–101 (2008).
14. W. R. Zipfel, R. M. Williams, R. Christie, A. Y. Nikitin, B. T. Hyman, and W. W. Webb, "Live tissue intrinsic emission microscopy using multiphoton-excited native fluorescence and second harmonic generation," Proc. Natl. Acad. Sci. U.S.A. **100**(12), 7075–7080 (2003).
15. I. W. Schie, C. Krafft, and J. Popp, "Applications of coherent Raman scattering microscopies to clinical and biological studies," Analyst (Lond.) **140**(12), 3897–3909 (2015).
16. J. Xu, L. W. Jiang, D. Y. Kang, X. J. Wu, M. F. Xu, S. M. Zhuo, X. Q. Zhu, J. B. Lin, and J. X. Chen, "Multiphoton imaging of low grade, high grade intraepithelial neoplasia and intramucosal invasive cancer of esophagus," Laser Phys. Lett. **14**(4), 045402 (2017).
17. S. Thomopoulos, J. P. Marquez, B. Weinberger, V. Birman, and G. M. Genin, "Collagen fiber orientation at the tendon to bone insertion and its influence on stress concentrations," J. Biomech. **39**(10), 1842–1851 (2006).
18. M. Sivaguru, S. Durgam, R. Ambekar, D. Luedtke, G. Fried, A. Stewart, and K. C. Toussaint, Jr., "Quantitative analysis of collagen fiber organization in injured tendons using Fourier transform-second harmonic generation imaging," Opt. Express **18**(24), 24983–24993 (2010).
19. P. S. Robinson and R. T. Tranquillo, "Planar biaxial behavior of fibrin-based tissue-engineered heart valve leaflets," Tissue Eng. Part A **15**(10), 2763–2772 (2009).
20. T. L. Sun, Y. Liu, M. C. Sung, H. C. Chen, C. H. Yang, V. Hovhannisyan, W. C. Lin, Y. M. Jeng, W. L. Chen, L. L. Chiou, G. T. Huang, K. H. Kim, P. T. C. So, Y. F. Chen, H. S. Lee, and C. Y. Dong, "Ex vivo imaging and quantification of liver fibrosis using second-harmonic generation microscopy," J. Biomed. Opt. **15**(3), 036002 (2010).
21. C. Bayan, J. M. Levitt, E. Miller, D. Kaplan, and I. Georgakoudi, "Fully automated, quantitative, noninvasive assessment of collagen fiber content and organization in thick collagen gels," J. Appl. Phys. **105**(10), 102042 (2009).
22. Z. Liu, K. P. Quinn, L. Speroni, L. Arendt, C. Kuperwasser, C. Sonnenschein, A. M. Soto, and I. Georgakoudi, "Rapid three-dimensional quantification of voxel-wise collagen fiber orientation," Biomed. Opt. Express **6**(7), 2294–2310 (2015).
23. Z. Liu, D. Pouli, D. Sood, A. Sundarakrishnan, C. K. Hui Mingalone, L. M. Arendt, C. Alonzo, K. P. Quinn, C. Kuperwasser, L. Zeng, T. Schnelldorfer, D. L. Kaplan, and I. Georgakoudi, "Automated quantification of three-dimensional organization of fiber-like structures in biological tissues," Biomaterials **116**, 34–47 (2017).
24. D. C. Lin, J. J. Hao, Y. Nagata, L. Xu, L. Shang, X. Meng, Y. Sato, Y. Okuno, A. M. Varela, L. W. Ding, M. Garg, L. Z. Liu, H. Yang, D. Yin, Z. Z. Shi, Y. Y. Jiang, W. Y. Gu, T. Gong, Y. Zhang, X. Xu, O. Kalid, S. Shacham, S. Ogawa, M. R. Wang, and H. P. Koeffler, "Genomic and molecular characterization of esophageal squamous cell carcinoma," Nat. Genet. **46**(5), 467–473 (2014).
25. K. Fakhrian, A. D. Ordu, F. Lordick, J. Theisen, B. Haller, T. Omrčen, M. Molls, C. Nieder, and H. Geinitz, "Long-term outcomes of trimodality treatment for squamous cell carcinoma of the esophagus with cisplatin and/or 5-FU: more than 20 years' experience at a single institution," Strahlenther. Onkol. **190**(12), 1133–1140 (2014).
26. K. Takubo, K. Sasajima, K. Yamashita, Y. Tanaka, and K. Fujita, "Prognostic significance of intramural metastasis in patients with esophageal carcinoma," Cancer **65**(8), 1816–1819 (1990).
27. E. Beaurepaire, M. Oheim, and J. Mertz, "Ultra-deep two-photon fluorescence excitation in turbid media," Opt. Commun. **188**(1), 25–29 (2011).
28. M. Makale, M. McElroy, P. O'Brien, R. M. Hoffman, S. Guo, M. Bouvet, L. Barnes, E. Ingulli, and D. Cheresh, "Extended-working-distance multiphoton micromanipulation microscope for deep-penetration imaging in live mice and tissue," J. Biomed. Opt. **14**(2), 024032 (2009).
29. G. McConnell, "Improving the penetration depth in multiphoton excitation laser scanning microscopy," J. Biomed. Opt. **11**(5), 054020 (2006).
30. W. F. Cheong, S. A. Prahl, and A. J. Welch, "A review of the optical properties of biological," IEEE J. Quantum Electron. **26**(12), 2166–2185 (1990).
31. R. Cicchi, D. Sampson, D. Massi, and F. Pavone, "Contrast and depth enhancement in two-photon microscopy of human skin ex vivo by use of optical clearing agents," Opt. Express **13**(7), 2337–2344 (2005).
32. K. Bahlmann, P. T. So, M. Kirber, R. Reich, B. Kosicki, W. McGonagle, and K. Bellve, "Multifocal multiphoton microscopy (MMM) at a frame rate beyond 600 Hz," Opt. Express **15**(17), 10991–10998 (2007).
33. T. Nielsen, M. Fricke, D. Hellweg, and P. Andresen, "High efficiency beam splitter for multifocal multiphoton microscopy," J. Microsc. **201**(3), 368–376 (2001).
34. M. Goetz, C. Fottner, E. Schirrmacher, P. Delaney, S. Gregor, C. Schneider, D. Strand, S. Kanzler, B. Memadathil, E. Weyand, M. Holtmann, R. Schirrmacher, M. M. Weber, M. Anlauf, G. Klöppel, M. Vieth, P. R. Galle, P. Bartenstein, M. F. Neurath, and R. Kiesslich, "In-vivo confocal real-time mini-microscopy in animal models of human inflammatory and neoplastic diseases," Endoscopy **39**(4), 350–356 (2007).

Biomedical Optics EXPRESS

35. K. Murari, Y. Zhang, S. Li, Y. Chen, M. J. Li, and X. Li, "Compensation-free, all-fiber-optic, two-photon endomicroscopy at 1.55 μm," Opt. Lett. **36**(7), 1299–1301 (2011).

1. Introduction

In surgeries for esophageal squamous cell carcinoma (ESCC), it is essential for the surgeons to completely remove the tumor tissue [1]. However, ESCC is often accompanied by intramural metastasis (IM), which is not easily detected preoperatively [2]. Recent studies have shown that IM occurs in 10-15% of advanced ESCC and such cases indicate a poor prognosis [3,4]. A study by Ide et al. recommended a 5-cm resection margin because most IMs are found in a distance less than 5 cm from the primary tumor [5]. Although this would have the potential to improve the clinical outcome of ESCC, more normal tissue will be removed than is required in a case of no IM, leading to an abnormal esophageal function. In order to determine a curative surgical margin, accurate detection of IMs by an advanced preoperative or intraoperative detection technique is necessary.

In the past few years, multiphoton microscopy (MPM) that relies on two-photon excited fluorescence (TPEF) and second harmonic generation (SHG) has experienced rapid growth in its application to cancer research [6–9]. By employing a near-infrared laser light, two photons are absorbed simultaneously to excite a fluorophore. Owing to the long wavelength and low energy of these photons, MPM can achieve deeper tissue penetration and minor phototoxicity. In particular, the major sources that are endogenous biomarkers include reduced nicotinamide adenine dinucleotide (NADH), flavin adenine dinucleotide (FAD), keratin, collagen, and elastin fibers. Together, these advantages make MPM suitable for label-free imaging of biological tissue. In this work, we attempted to evaluate whether MPM has the ability to identify IM in the esophageal wall. IM in esophageal cancer consists of a metastatic lesion from the primary tumor to the esophageal wall without intraepithelial cancer extension. It has also been reported that IMs in ESCC are caused by lymphatic invasion to the submucosal layer [10]. To histologically detect IMs by MPM, the submucosal tumor was identified to be an IM of ESCC according to this definition. Figure 1 shows a morphological diagram of IM in the esophageal wall, and the position of IM was our region of interest.

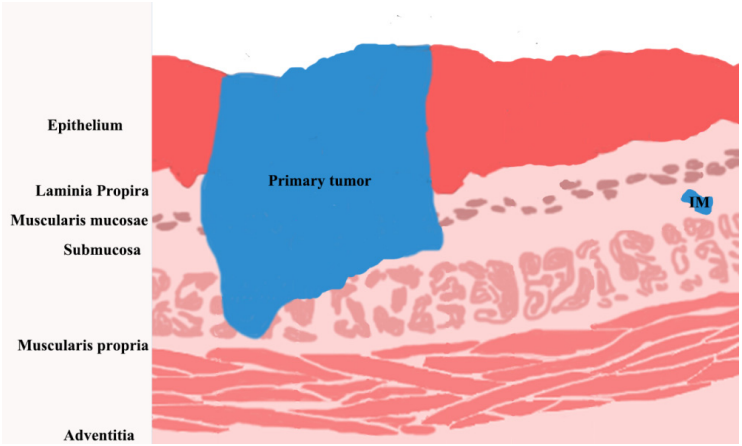

Fig. 1. Morphological diagram of IM in the esophageal wall.

For label-free identification of IMs in the esophagus, unstained frozen sections of human esophageal tissue obtained from surgically excised tissue were analyzed. Until now, routine hematoxylin and eosin-stained (H&E-stained) tissue remains the gold standard for definitive esophageal cancer diagnosis. Therefore, corresponding H&E-stained sections were also prepared for confirmation of IM. To our knowledge, this is the first examination of MPM features of intramural esophageal metastases that could lead to further studies in intact tissue.

Biomedical Optics EXPRESS

2. Materials and methods

2.1 Tissue sample preparation

Informed written consent for this research was obtained from each patient before the procedure, and the Institutional Review Board of the Affiliated Union Hospital approved this study. Resected specimens were obtained far from the primary tumor, at a distance of 1-5 cm, from 34 patients with squamous cell carcinoma (SCC) of the esophagus. The fresh tissue blocks were immediately sent from the operating room to the pathology laboratory after resection, were embedded in an optimal cutting temperature (OCT) compound, and were frozen in a freezing microtome. Then, the frozen blocks were sectioned into five serial frozen sections (one with 5-μm thickness and the others with 10-μm thickness) perpendicular to the esophageal layers. The middle one (5-μm thickness) that was reviewed by experienced pathologists was stained with H&E and four samples were confirmed with IM. The rest of the frozen sections of these four samples were using for two-dimensional (2D) MPM imaging. In addition, the corresponding tissue blocks of these four samples were also sectioned into five serial frozen sections (30-μm thickness) parallel to the esophageal layers for 3D MPM imaging. Figure 2 shows a diagram for preparation of the frozen sections. Once the frozen sections were prepared, they were sent to the multiphoton laboratory, using a standard pathologic transport container for MPM imaging that day. If the sections were obtained too late, they were stored in a refrigerator at −80°C and were imaged the next day. The clinicopathological characteristics of these four patients are shown in Table 1. However, the number was too small to perform a more rigorous evaluation. More samples will be collected in a future study.

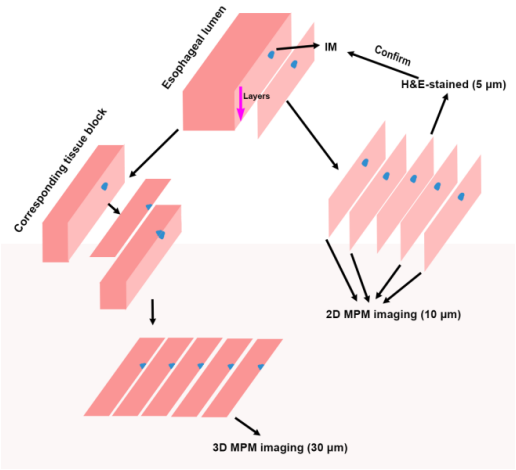

Fig. 2. A diagram outlining the preparation of frozen sections.

Table 1. The clinicopathological characteristics of four patients with squamous cell carcinoma

	Gender	Age	Depth of primary tumor invasion	Residual tumor	Intramural Metastasis		
					Location	Distance from Primary tumor (cm)	Size (mm × mm)
1	male	55	muscularis propria	R0	Lt	2.2	5.0 × 3.0
2	female	67	submucosa	R0	Lt	1.5	3.5 × 2.5
3	female	63	muscularis propria	R0	Ut	1.6	2.7 × 2.5
4	female	52	muscularis propria	R0	Lt	2.4	2.4 × 1.8

R0: no residual tumor, Lt: lower thoracic, Ut: upper thoracic

Biomedical Optics EXPRESS

2.2 Label-free multiphoton imaging

Before MPM imaging, the sections were submerged in a phosphate-buffered saline solution to avoid dehydration and covered with coverslips. Then, the samples were put onto an optional HRZ 200 fine-focusing stage (HRZ 200; Carl Zeiss, Inc.) of the system for imaging. The commercial microscope (Zeiss LSM 510 META, Jena, Germay) equipped with a mode-locked femtosecond Ti: sapphire laser (tuning range of 700-980 nm, Mira 900-F; Coherent, Inc.) used in this work has been described elsewhere [11]. Here, an oil immersion objective (Plan-Apochromat 63 × , N.A. 1.4; Zeiss) was used for collecting the backscattered signals. Then, the signals were directed to the META detector. Two separate channels were used to record the SHG signals (387-419 nm, green color-coded) and TPEF signals (430-710 nm, red color-coded). The exciting power was 5-10 mw and the excitation wavelength was 810 nm. The scan time for a 2D image was 1.57 s and the measured resolution was 0.29 μm per pixel.

3. Results

3.1 2D optical identification of IM in the esophageal wall

To investigate whether MPM had the potential to histologically identify IMs in the esophageal wall, longitudinal frozen sections perpendicular to the esophageal layers were imaged. Figure 3 showed the representative MPM image and corresponding H&E-stained image of full-thickness esophageal tissue with an IM in the submucosa. Figure 3(a) and 3(b) consisted of the TPEF and SHG images, respectively. In Fig. 3(c), each layer of the esophageal wall and the interfaces between the layers were clearly differentiated because the endogenous signals of the adjacent layer were different. Hence, the position of the submucosa was easily discernible. The submucosa was mainly made up of fibrous tissue that was marked by green, red, or yellow colors (the overlay of green and red colors). In the fibrous tissue, an IM (arrow) that was composed of abnormal cells (red color) was found. However, the normal structure of the esophageal mucosa, which consisted of stratified squamous epithelium, lamina propria, and muscularis mucosae, was still maintained. The corresponding H&E-stained image shown in Fig. 3(d) displayed the same details as the MPM images.

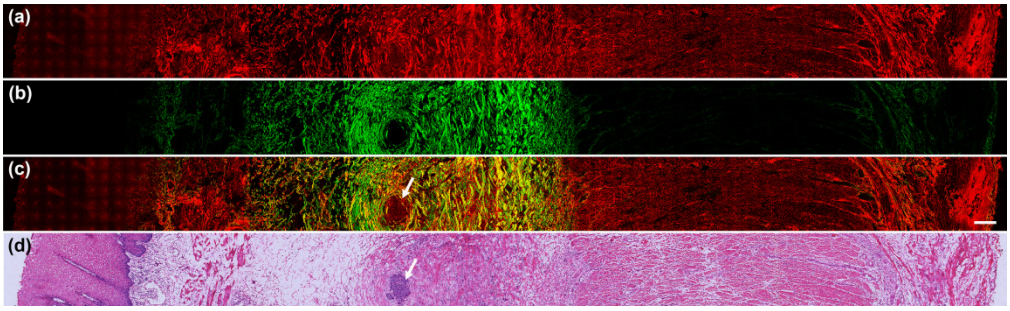

Fig. 3. Representative MPM images and corresponding H&E-stained image of full-thickness esophageal tissue with an IM in the submucosa. (a) TPEF image; (b) SHG image; (c) Overlay of TPEF and SHG image; (d) H&E-stained image (magnification, 40 ×). Arrow: IM; scale bar: 200 μm.

Nevertheless, more detailed cytological information about the IM should be obtained by MPM. Previous studies have shown that MPM has a resolution comparable to that of routine H&E-stained images [12–14]. In order to better identify the IM and distinguish between the IM and surrounding fibrous tissue, a higher magnification view of the IM region and surrounding fibrous tissue is presented in Fig. 4. Figures 4(a) and 4(b) consisted of the TPEF and SHG images, respectively. As shown in Fig. 4(c), the fibrous tissue consisted of collagen fiber and elastic fiber. The collagen fiber was detected by SHG signals (star) or SHG/TPEF signals (arrowhead), while the elastic fiber (arrow) was identified via TPEF signals. Even so,

Biomedical Optics EXPRESS

the fibrous tissue was primarily discerned by the SHG signals of the collagen fiber since it has a non-centrosymmetric molecular structure that is suitable for generating SHG signals [15]. The IM, which had an obvious cellular structure, consisted of a mass of tumor cells (triangle) with different shapes and sizes, making it easily distinguishable from the surrounding fibrous structure. In particular, the tumor cells produced TPEF signals, while the surrounding tissues not only emitted TPEF signals but also produced SHG signals. Otherwise, the TPEF signals of the tumor cells were emitted by structural proteins, NADH, and FAD, leading to further identification of the IM among the fibrous tissue. Although the corresponding H&E-stained image in Fig. 4(d) was consistent with the MPM image, the fibrous tissue in the H&E-stained image was not well discerned. This ability to identify fibrous tissue was an advantage of MPM imaging when compared to routine H&E-stained images. These results show that MPM cannot only histologically identify an IM, but also qualitatively analyze the difference between the IM and surrounding fibrous tissue. Owing to the different endogenous components of an IM and surrounding fibrous tissue, spectral imaging was also performed. The spectra of the region of interest and the corresponding cover glass were obtained under the same condition. The final spectra were obtained by the spectra of the region of interest minus the spectra of the corresponding cover glass. After the subtraction of this background, the averaged normalized multiphoton emission spectra of the IM and surrounding fibrous tissue of the four patients are shown in Fig. 4(e). The endogenous signals of each peak of cells and fibers had been described in detail in our previous work [16]. Briefly, the main components of the surrounding fibrous tissue were collagen fibers (405 nm) and elastic fibers (510 nm), while those of the IM were structural proteins, NADH and FAD (510, 475, 535 nm), of the tumor cells. This obvious difference in the emission spectra at 405 nm indicated that MPM could be used for spectral discrimination between an IM and surrounding tissue, thus effectively identifying the boundary between them. The boundary was indicated by white circles, both in the SHG image and the overlay of the TPEF and SHG images.

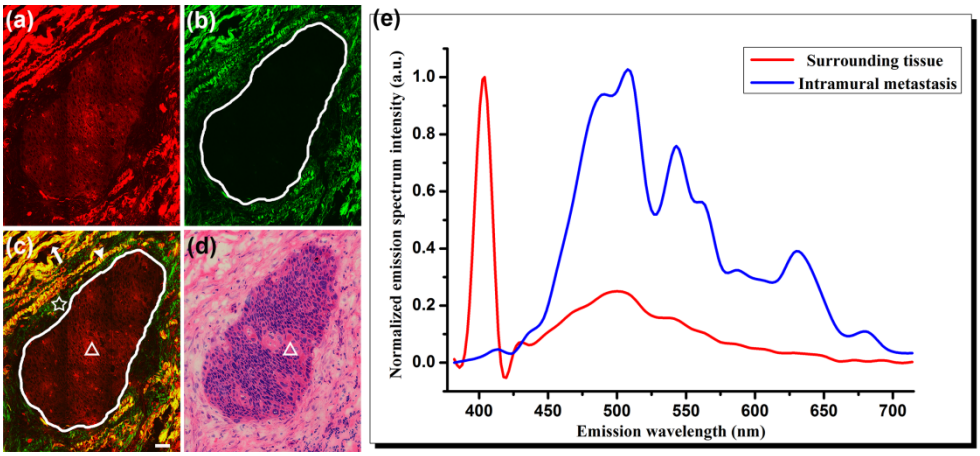

Fig. 4. Higher magnification view of the region of the IM and surrounding fibrous tissue and their averaged normalized multiphoton emission spectra. (a) TPEF image; (b) SHG image; (c) Overlay of TPEF and SHG image; (d) H&E-stained image (magnification, 40 ×); (e) Normalized multiphoton emission spectra. Star: collagen fiber detected by SHG signals; arrowhead: collagen fiber was detected by SHG/TPEF signals; arrow: elastic fiber identified via TPEF signals; triangle: tumor cells; scale bar: 50 μm.

3.2 3D optical imaging of IM

In addition to allowing histological identification of the region of IM similar to routine H&E-stained images, MPM clearly imaged the fibrous tissue and spectrally identified the boundary between the IM and surrounding tissue. However, these processes were accomplished using a 2D method. A future clinical application should be performed by 3D optical imaging. In order

Biomedical Optics EXPRESS

to further investigate whether MPM can be used for 3D optical imaging of an IM, Z-stack imaging was performed at Z intervals of 1 μm, and a maximum penetration depth of 25 μm was acquired. A Z-stack of MPM images, which is shown in Fig. 5, was obtained at a scan time of 39.25 s and was an orthogonal view giving the XY, XZ, and YZ plane on a certain spot. Figure 5(a) and 5(b) show the TPEF and SHG images, respectively. By moving the green, red, and blue lines in Fig. 5(c), the section plane can be positioned at any XYZ coordinate of the Z-stack, leading to an accurate identification of the position of the IM. The XY plane showed one of the 2D images of the stack. Similar information to Fig. 4(c) was also acquired, including collagen fiber that emitted SHG signals (star) and SHG/TPEF signals (arrowhead), elastic fiber (arrow) that produced TPEF signals, and tumor cells (triangle). The region of the IM in the three planes was marked by a white circle. In the XZ and YZ planes, the precise thickness of the IM in the Z-direction could be described. However, this image just showed part of the IM since the penetration depth was limited. If the excitation light can penetrate the whole layers of the esophageal wall, it can be foreseen that the histological image of the IM in the esophageal wall similar to Fig. 3(c) will be shown in the XZ plane. These results indicated that 3D identification of the region of IM in esophageal tissues is possible by Z-stack imaging.

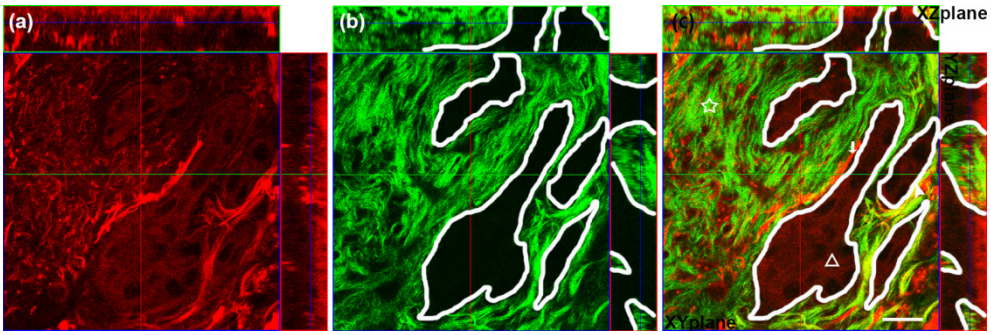

Fig. 5. Orthogonal view of a Z-stack image of an IM. (a) TPEF image; (b) SHG image; (c) Overlay of TPEF and SHG image. Star: collagen fiber detected by SHG signals; arrowhead: collagen fiber was detected by SHG/TPEF signals; arrow: elastic fiber identified via TPEF signals; triangle: tumor cells; white circle: IM; scale bar: 20 μm.

3.3 3D fiber orientation and 3D directional variance for assisted identification of IM

As mentioned above, MPM had the advantage of imaging fibrous tissue surrounding the IM, especially collagen fibers, when compared to routine H&E-stained images. Therefore, our study wanted to present this advantage in a quantitative manner since many groups have shown that unwanted changes in collagen fiber architecture provide a potential biomarker for diagnosing diseases or injuries [17–21]. Here, we investigated whether there was any alteration in the collagen fibers surrounding the IM compared to collagen fibers in normal submucosa. The 3D fiber orientation and 3D directional variance of collagen fibers surrounding the IM and collagen fibers in normal submucosa were measured by using a 3D-weighted orientation vector summation technique that was reported in a study by Liu et al. [22,23]. They defined two angles (φ and θ) to depict 3D fiber orientation, as shown in Fig. 6(a). They also indicated that a higher value of 3D directional variance indicated more random fiber arrangement and a lower one showed more highly aligned fibers. In our study, two normal areas and two areas containing collagen fibers surrounding the IM of each patient were calculated. The 3D reconstruction of the collagen fibers in normal submucosa and the collagen fibers surrounding the IM are shown in Figs. 6(b) and 6(c), respectively. By applying this technique to these two types of 3D stacks, φ and θ distributions of the normal case (Figs. 6(d) and 6(e)) and IM case (Figs. 6(f) and 6(g)) were obtained. The φ distribution of the two cases showed a peak at approximately 90°, indicating that most of the fibers were

Biomedical Optics EXPRESS

parallel to the XY plane. The θ distribution of the normal case showed two peaks at approximately 40° and 140°, indicating that two main orientations of the fibers dominated the alignment. However, the θ distribution of the IM case presented one peak at approximately 60°, corresponding to one preferred orientation of most fibers. In Fig. 6(h), the value of the 3D directional variance of the normal case (0.873 ± 0.003, n = 8) was higher than that of IM case (0.727 ± 0.001, n = 8). These results showed that the collagen fibers in the IM case were more aligned than that in the normal case. The arrangement of collagen fibers during 3D identification of an IM in the submucosa may be used as a biomarker for diagnoses of IMs.

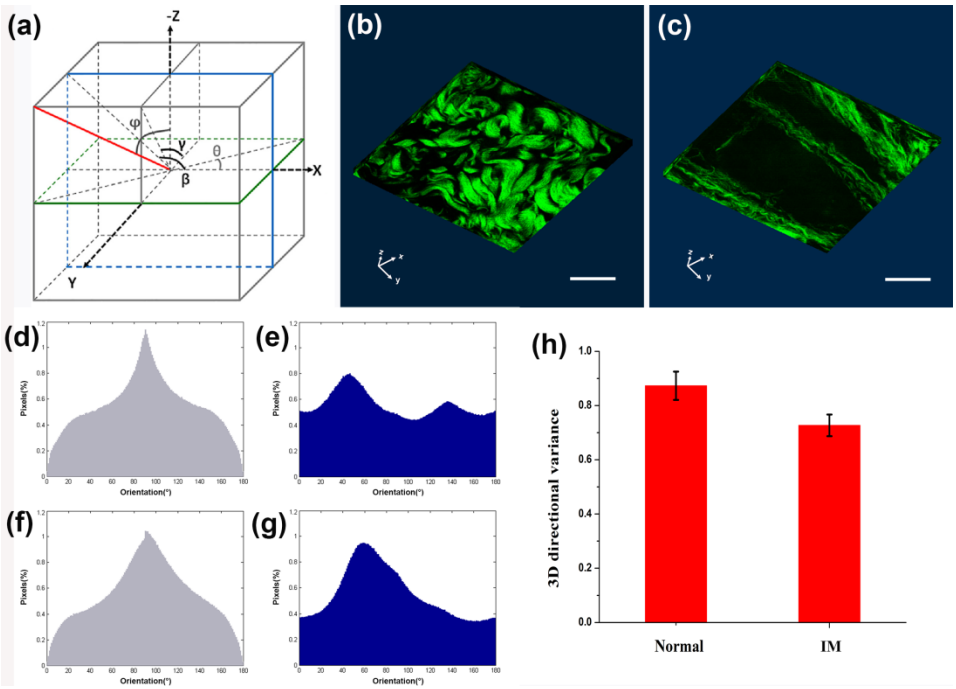

Fig. 6. 3D fiber orientation and 3D directional variance of collagen fibers surrounding the IM and collagen fibers in normal submucosa. (a): Two angles (φ and θ) that depict 3D fiber orientation [23]; (b) 3D reconstruction of a collagen fiber in normal submucosa; (c) 3D reconstruction of a collagen fiber surrounding the IM; (d): φ distribution of normal case; (e) θ distribution of normal case; (f) φ distribution of IM case; (g): θ distribution of IM case; (h) 3D directional variance. Scale bar: 20 μm.

4. Discussion

Cancer of the esophagus, predominantly ESCC, is one of the most common types of gastrointestinal cancer worldwide and especially in China, where it is the fourth leading cause of cancer-related deaths [24]. Although several treatment strategies were introduced, surgery is considered the mainstay of ESCC treatments. However, the total outcome was still poor with a ten-year survival rate of less than 15% [25]. This is due to the recurrence of ESCC originating from residual cancer cells. Even if the resection margins were clean, subepithelial lesions, such as IMs, may remain beyond the margins [1]. In addition, the prognosis of ESCC with an IM was much poorer than for that without an IM.

The presence of an IM is considered the typical pathway for tumor spread in ESCC. IMs are often detected in the submucosal layer without intraepithelial spread and with a frequent erosion or ulceration. Previous literature depicted that erosion or ulceration was observed in 42.9% of the detected cases [26]. However, with the absence of erosion or ulceration, a preoperative diagnosis of IM is difficult. In addition, an IM is often observed inside the esophageal wall far from the primary lesion and the size is small in some cases. To determine

Biomedical Optics EXPRESS

the line of dissection of the esophagus during surgery, all IMs should be detected preoperatively. In these cases, a new preoperative or intraoperative detection technique should be introduced. Hence, MPM was used to study IMs in the submucosa of esophageal tissue.

In our present study, we demonstrated the ability of MPM to histologically identify an IM and surrounding fibrous tissue based on SHG and TPEF signatures. Furthermore, the emission spectra of an IM and fibrous tissue could be used to discern the boundary between them. To evaluate whether MPM had the potential to generate 3D images of an IM, 3D imaging of the IM region was also performed. Lastly, the differences between normal collagen fibers and the collagen fibers around an IM were quantitatively analyzed, since the structural changes in collagen fibers may be a potential biomarker for diagnosing cancer.

It is important to note that our results were obtained with frozen sections. Some limitations must be overcome before MPM can be integrated into current clinical practice. For example, the thickness of the esophageal wall with an IM was approximately 6-10 mm, and the IM was often in the submusosal layer at distance of 1.5-3 mm to the surface in this study. This typical position of an IM rendered the need for a technique with high-penetration depth. Since multiphoton microscopy was first introduced, many groups devoted themselves to increasing the penetration depth by different changes in the work path. Because the maximum penetration depth is usually limited by the amount of laser power, the laser repetition rate that can redistribute the laser power was optimized in a study by Beaurepaire et al. [27]. A study by Makale reported an MPM system acquiring a penetration depth of 750 to 800 μm by incorporating high-NA, long-working-distance, water-dipping lenses [28]. Equipped with a passive predispersion compensation system, MPM achieved more than a threefold increase in penetration depth [29]. Because the penetration depth in biological tissue is also commonly limited by scattering produced by turbid media [30], biocompatible optical clearing agents, which can reduce scattering enhanced contrast and thus increase penetration depth, were applied [31]. Though the penetration depth in skin is almost 150 to 200 μm now, the detection of IMs in the esophagus might be possible in the future. There are other challenges that must be overcome, including the total cost of the technique and motions during the surgery. However, this technique has been improved at a rapid pace, including the development of multifocal multiphoton microscopy [32, 33], a miniaturized multiphoton endoscope system [34], and an inexpensive fiber-optic scanning multiphoton endomicroscope [35]. Every effort has been made to facilitate the clinical application of MPM.

In summary, this study showed that MPM has the potential ability to detect an IM and identify the boundary between an IM and fibrous tissues. It is expected that MPM can be used in clinical research in the future with the development of a new MPM endoscope system.

Funding

National Natural Science Foundation of China (Grant No. 81671730, 81271620), National Key Basic Research Program of China (2015CB352006), Joint Funds of Fujian Provincial Health and Education Research (WKJ2016-2-28), Program for Changjiang Scholars and Innovative Research Team in University (IRT_15R10).

Acknowledgments

The authors thank Qun Zhou for measuring the 3D fiber orientation and 3D directional variance.